Materials Research Bulletin 47 (2012) 1158–1163

Contents lists available at SciVerse ScienceDirect

Materials Research Bulletin

journal homepage: www.elsevier.com/locate/matresbu

Crystal field effect on the effective magnetic moment in A_2CoWO_6 (A = Ca, Sr and Ba)

C.A. López [a,b], M.E. Saleta [a,b,c], J. Curiale [a,b,c], R.D. Sánchez [a,b,c,*]

[a] Centro Atómico Bariloche, Comisión Nacional de Energía Atómica, Avenida Bustillo 9500, 8400 S. C. de Bariloche, RN, Argentina.
[b] Consejo Nacional de Investigaciones Científicas y Técnicas – CONICET, CCT-Comahue, Quintral 1250, 8400 S. C. de Bariloche, RN, Argentina.
[c] Instituto Balseiro, Comisión Nacional de Energía Atómica and Universidad Nacional de Cuyo, Avenida Bustillo 9500, 8400 S. C. de Bariloche, RN, Argentina.

ARTICLE INFO

Article history:
Received 16 November 2011
Received in revised form 27 January 2012
Accepted 3 February 2012
Available online 10 February 2012

Keywords:
A.Oxides
D. Magnetic properties

ABSTRACT

We prepared the antiferromagnetic Ca_2CoWO_6, Sr_2CoWO_6 and Ba_2CoWO_6 double perovskites with different crystalline structures, which are monoclinic, tetragonal and cubic respectively. The crystalline structures affect the Co–O distances and the local octahedral symmetry. Magnetic susceptibility experiments were performed as a function of magnetic field and temperature. We found that the effective magnetic moment (μ_{eff}) of Co^{2+} is partially unquenched and we also found that μ_{eff} increases with the average of Co–O distances that form the CoO_6 octahedra. A simple model associates the behavior of the effective magnetic moment with crystal field effects.

1. Introduction

The revival of interest in the double perovskite family was triggered by reports on the ferromagnetic Sr_2FeMoO_6 [1–3], demonstrating that in the electronic structure only minority and polarized spins are present at the Fermi level. This material was shown to exhibit intrinsic tunnelling-type magnetoresistance at room temperature [4]. The spin-polarized transport in these materials is an actual topic of intensive research, due to its potential for application in spintronics and magnetoelectronic devices [5,6].

Antiferromagnetic A_2CoBO_6 double perovskites are important to produce more complex systems as spin valves [7] and others that use exchange bias (EB) mechanism [8] reducing the mismatch effect with the ferromagnetic parents. The A_2CoWO_6 (with A = Ca, Sr or Ba) family call our attention as antiferromagnetic candidates due to their crystalline versatility. Their crystalline structures were reported as monoclinic, tetragonal and cubic respectively [9–12].

As these double perovskites are obtained under an oxidative atmosphere, the more probable electronic configuration of the ions are $Co^{2+}(3d^7)$ and $W^{6+}(4d^0)$ being the cobalt the only magnetic ion. In general, the transitions metal ions have effective magnetic moments that can be described by a spin-only configuration due to the quenched orbital moment. In this particular case the magnetic moment of the Co^{2+} ions for the high spin configuration ($S = 3/2$) should be $3.87\mu_B$. However, only one work on Sr_2CoWO_6 reported quenched orbital moment ($3.02\mu_B$) [12] and they suggest that the magnetic moment (μ_{eff}) value depend of the external magnetic field value. But, high fields magnetic studies in Co double perovskite are very scarce in the literature. Other double perovskites with Co^{2+} ions present orbital contribution to the effective magnetic moment and sometimes the μ_{eff} value is sensitive to the disorder in the samples induced by different chemical routes [13].

In this work we study how to change the magnetic effective moment with temperature and magnetic field for the A_2CoWO_6 double perovskite with A = Ca, Sr and Ba. A model developed to describe the magnetic susceptibility of Co^{2+} ions in Tutton salts [14] has been applied to describe the variations of the effective magnetic moment in the double perovskites, which can be explained by crystal field effects due to the variation of the distances between the oxygen environment and the Co^{2+} ions.

2. Results

2.1. Synthesis and structural characterization

A_2CoWO_6 (A = Ca, Sr and Ba) were prepared by solid-state reaction. Stoichiometric analytical grade amounts of ACO_3, $CoCO_3$ and WO_3 were mixed, ground, placed in a platinum crucible and treated at 600 °C in air for 24 h. The resulting powder was reground and calcined at 800 °C and 1000 °C for 24 h in each step. Finally the products were fired at 1150 °C for 24 h with intermediate milling

* Corresponding author at: Centro Atómico Bariloche, Comisión Nacional de Energía Atómica, Avenida Bustillo 9500, 8400 S. C. de Bariloche, RN, Argentina. Tel.: +54 (294) 4445158; fax: +54 (294) 4445274.
E-mail address: rodo@cab.cnea.gov.ar (R.D. Sánchez).

0025-5408/$ – see front matter © 2012 Elsevier Ltd. All rights reserved.
doi:10.1016/j.materresbull.2012.02.008

Table 1
Average of Co–O and Co–Co main distances, μ_{eff} and θ values obtained adjusting the χ^{-1} vs. T data at H =5 and 50 kOe with a Curie–Weiss law between $200 < T(K) < 300$. The numbers between parenthesis are the error of the last significative digit. Also, are the best model parameters: λ, α, α' and D, used to describe the μ_{eff} vs. T curves at 5 and 50 kOe.

	Ca_2CoWO_6	Sr_2CoWO_6	Ba_2CoWO_6
⟨Co–O⟩ (Å)	2.093(2)	2.064(2)	2.129(2)
⟨Co–Co⟩ (Å)	7.7591(3)	7.9225(3)	8.1080(3)
$\mu_{eff}(\mu_B)$ (5/50 kOe)	5.14(1)/5.01(1)	5.07(1)/4.89(1)	5.18(1)/5.13(1)
$-\theta$(K) (5/50 kOe)	68(2)/61(2)	57(2)/56(2)	41(2)/52(2)
λ (cm^{-1})	−143	−143	−143
α (5/50 kOe)	1.460/1.350	1.455/1.256	1.450/1.345
α' (5/50 kOe)	1.572/1.485	1.700/1.485	1.405/1.255
D (cm^{-1})	487	557	0

of the reaction mixture. The rate of heating was of 5 °C min^{-1} and the furnace was switched off after each step.

The identification and characterization of the phases were carried out by X-ray powder diffraction (XRPD) using a Rigaku D-MAX-IIIC diffractometer with Cu Kα (λ = 1.5418 Å) radiation. The 2θ range was from 10° up to 70° with increments of 0.02° and the counting time was 4 s/step. The experimental patterns were analyzed with the Rietveld method. Those XRPD patterns are characteristics of perovskite structure. The space group (S.G.) for Ca_2CoWO_6 is $P21/n$, for Sr_2CoWO_6 is $I4/m$ and for Ba_2CoWO_6 is $Fm3m$. Minor amounts of non-magnetic impurities were detected and included in the refinements: 0.5% of $CaWO_4$ in Ca_2CoWO_6; 0.2% of $SrWO_4$ in Sr_2CoWO_6; 1.2% of Ba_2WO_5 and 0.2% of BaO in Ba_2CoWO_6. From the fit of the XRPD pattern, the calculated average distances between two neighbor cobalt atoms (⟨Co–Co⟩) and between cobalt and oxygen atoms (⟨Co–O⟩) for each compounds are presented in Table 1.

2.2. Magnetic susceptibility

The magnetic measurements were performed in a commercial superconducting quantum interference device (SQUID, Quantum Design MPMS 5T) magnetometer in the $5 \leq T(K) \leq 300$ temperature range, with different magnetic fields up to 50 kOe.

In Fig. 1 we show M vs. T curves of the A_2CoWO_6 family. Each plot shows M curves at H = 5, 10, 30 and 50 kOe. In all the cases, a maximum of magnetization is observed at T_N (Néel temperature) which is associated with the appearance of antiferromagnetic long range order. Practically, no magnetic field dependence of T_N was observed considering ±1 K of uncertainty.

The obtained T_N values are: 33(1), 24(1) and 18(1) K for Ca_2CoWO_6, Sr_2CoWO_6 and Ba_2CoWO_6 respectively which are in good agreement with the previous reported data of magnetization (A = Sr and Ba) [10–12] and neutron diffraction data (for A = Ca) [9]. In Fig. 2, T_N is plotted as a function of the average ⟨Co–Co⟩ distance (see Table 1). The diminution of the A cation size (r_A) introduces more structural distortion and consequently reduces the effective ⟨Co–Co⟩ distance. The maximum T_N is achieved for the monoclinic and more distorted Ca_2CoWO_6 compound with the lower ⟨Co–Co⟩ distance.

In order to characterize the paramagnetic phase at high temperature and to analyze the A cation size influence on the magnetic properties, we study the inverse of the susceptibility taken as the $\chi^{-1} = H/M$ ratio (see Fig. 1). For this Co^{2+} case, the inverse of the magnetic susceptibility is not completely linear with temperature in the paramagnetic region, $T_N < T < 300$ K. We detect a small field dependence and we have not detected any ferromagnetic spurious phase in the samples.

In the bottom of Fig. 1 we only present the χ^{-1}–T curves at H = 5 and 50 kOe respectively to visualize more clearly the linear deviation. In order to make a comparative analysis between the

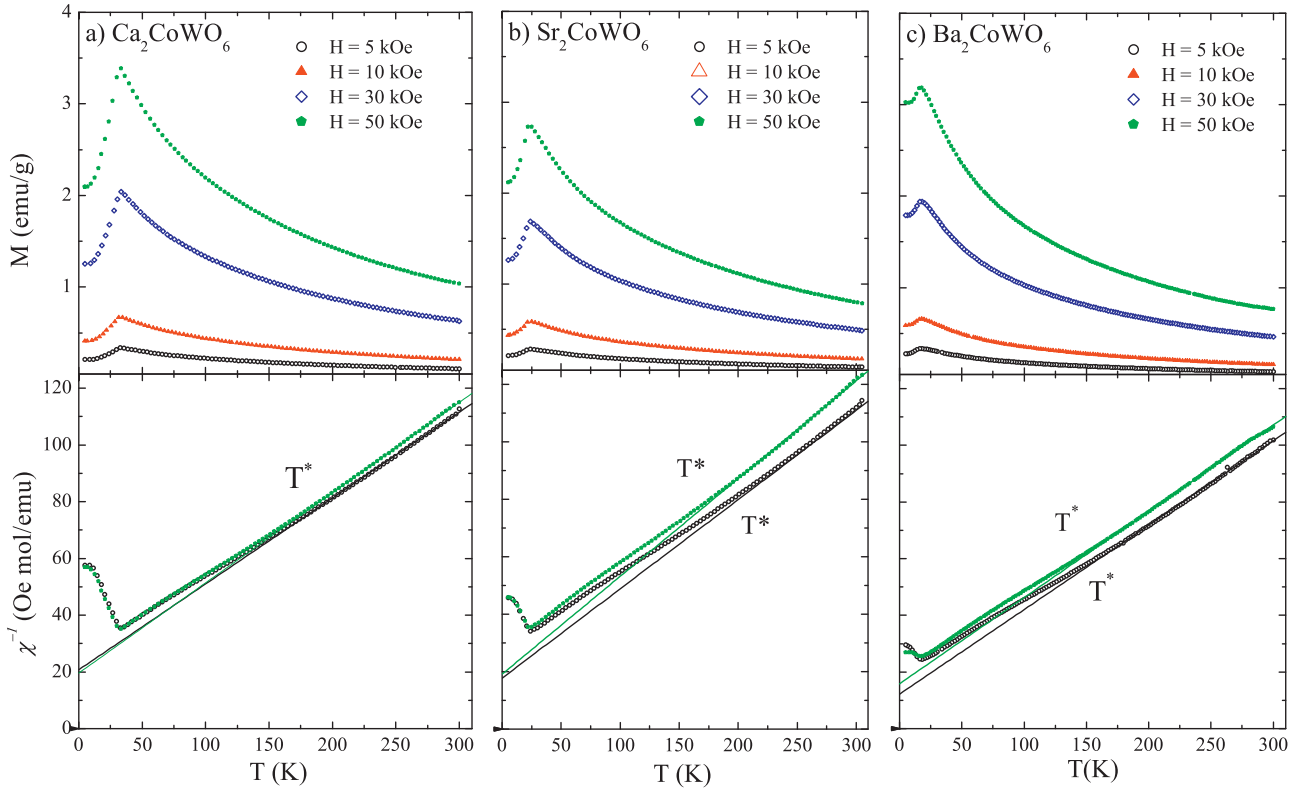

Fig. 1. On the top, magnetization (M) as a function of temperature (T) data taken with different magnetic field. On the bottom, inverse of the magnetic susceptibility as a function of temperature for (a) Ca_2CoWO_6, (b) Sr_2CoWO_6 (c) Ba_2CoWO_6 at 5 and 50 kOe.

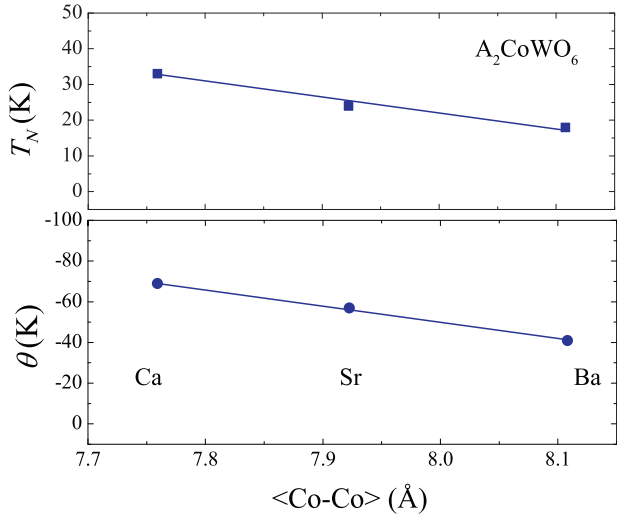

Fig. 2. Top: Néel temperature (T_N), bottom: Curie–Weiss temperature (θ) as a function of Co–Co distance for different A cation (θ values are obtained from the adjust with the Curie–Weiss law to the 5 kOe experiment at high temperature).

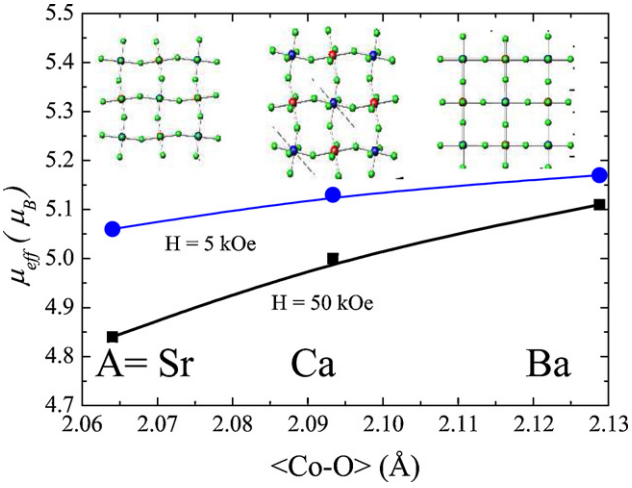

Fig. 3. μ_{eff} vs. ⟨Co–O⟩ at 300 K for different A cations and H (5 and 50 kOe). In the top are the crystalline structure schemes.

compounds, we take only the data of the measured curves at different H above 200 K and we fitted these curves with the Curie–Weiss law ($\chi = C/T - \theta$). Where C and θ are the Curie constant and Curie–Weiss temperature respectively. At 5 kOe the θ values in K are -68 ± 2, -57 ± 2 and -41 ± 2, for A = Ca, Sr and Ba respectively, which are also plotted in Fig. 2 (see bottom of the figure). Both, θ and T_N present similar correlations with the ⟨Co–Co⟩ distance and the negative values confirm the antiferromagnetic character of the interactions in these compounds. The absolute θ/T_N ratio is larger than 1, which suggests that first and second neighbor interactions among the Co^{2+} are present. This was previously confirmed by low-temperature neutron diffraction studies on A_2CoWO_6 [9–11] where the antiferromagnetic ordered is second kind as in CoO archetype.

Our experimental effective magnetic moment of $\mu_{eff} = 5.14 \pm 0.01$, 5.07 ± 0.01, $5.18 \pm 0.01 \mu_B$ for A = Ca, Sr and Ba respectively, are slightly lower than previously reported for Sr_2CoWO_6 (5.20μ_B) and Ba_2CoWO_6 (5.58 μ_B) [10,11]. Also, other related compounds as $(Sr,Ba)_2CoMoO_6$, $(Sr,Ba)_2CoUO_6$ and $(Ca,Sr)_2CoTeO_6$ also show effective moments well above that spin-only magnetic moment [11,15–19]. As the oxidation state of wolfram ions is +6 and it is a $5d^0$ or closed shell that does not contribute to the paramagnetism, the experimental μ_{eff} is completely associated with Co^{2+}. The values obtained are larger than the spin-only (μ_S) but these do not reach the expected value for the pure spin–orbit contribution ($\mu_J = 6.63\mu_B$) case.

Also, from the inverse of susceptibility plots it is observable small differences at higher temperatures when the magnetic field is changed (see bottom of Fig. 1). To visualize these changes easily, the μ_{eff} and θ obtained from the Curie–Weiss fits at two different magnetic fields for the different A cations are shown in Table 1. The μ_{eff} value slightly decreases when the magnetic field is increased (from 5 to 50 kOe) for all the samples (see Fig. 3). In particular, μ_{eff} decreases around 3.5% for the Sr case and 1% for the Ba double perovskite. On the other hand, we expect that μ_{eff} should have some correlation with r_A. However, μ_{eff} increases in the Sr, Ca and Ba sequence, fact that we will try to explain in the following section.

3. Discussion

The octahedral local symmetry around the Co^{2+} ions is modified by the different crystalline structures in the three compounds. The Ba double perovskite has a perfect octahedra with O_h symmetry where the six Co–O distances are equal. On the other hand, Sr presents a reduction of the local symmetry, it is lowered to tetragonal (D_{4h}), where the four Co–O distances in the octahedral plane are equivalent while the axial Co–O distances present different values. Also, in the more structurally distorted distances, three different Co–O characteristics distances are observed; however the Co–O equatorial plane distances are practically equal, resulting in a quasi D_{4h} tetragonal symmetry. These different octahedral oxygen environments around the magnetic ion should modify the crystal field, which will change the structure of energy levels of Co ions and consequently their magnetic susceptibility. Also, these different crystalline structures with different octahedra spatial arrangement affect the average Co–Co distance modifying the strength of the magnetic interactions.

The μ_{eff} values obtained from the χ^{-1} vs. T fit data at $H = 5/50$ kOe are in Table 1 for the Ba, Ca and Sr cases. The evolution of μ_{eff} as a function of the average ⟨Co–O⟩ distance for each compound can be clearly observed in Fig. 3. This plot shows the correlation between μ_{eff} with the oxygen environments around the Co ions. Although, the lower Co environment symmetry corresponds to the Ca compound, the shorter Co–O distances and the lower μ_{eff} value are in the Sr case. This graph shows directly how the μ_{eff} is principally affected by the Co–O distance than the crystalline distortion. It is remarkable that Sr_2CoWO_6 double perovskite presents the lowest μ_{eff} value, following by Ca_2CoWO_6, and finally the highest μ_{eff} data corresponds to the Ba_2CoWO_6 compound. As we mentioned before, the Ba compound has cubic field and it presents perfect octahedral environment of oxygen around the Co (O_h symmetry). While the lowest magnetic moment is for Sr_2CoWO_6 where the local symmetry is reduced to D_{4h}. For Ca_2CoWO_6, although both Co–O distances [9] at the equatorial plane are different, 2.103(2) Å and 2.114(2) Å, for the magnetic calculations the local symmetry can be considered similar to D_{4h} with axial symmetry. To corroborate this hypothesis, we will treat to estimate the behavior of the effective magnetic moment with the distortion of the local crystal field for the different A ions in the double perovskite system A_2CoWO_6.

3.1. The model

The Co^{2+} free ion possesses a $3d^7$ electronic configuration, whose ground state is ^4F and above this is the ^4P state at approximately 22,500 cm^{-1}. When the Co^{2+} ion is introduced in the octahedral oxygen environment, the cubic ligand field (O_h) from the bottom, splits into two triplets orbitals (T_{1g} and T_{2g}) and one singlet state (A_{2g}) where T_{1g} is the lowest [20]. The excited T_{2g}

and A_{2g} states are over 8000 cm^{-1} and they are not thermally populated at room temperature. First order orbital moment together with spin orbital moment split the ground state T_{1g} into a sextet ($J = 5/2$), a quadruplet ($J = 3/2$) and a doublet ($J = 1/2$) and this last one being the lowest, which are completely separated by first and second order Zeeman effects. The magnetic susceptibility can be computed as a function of the perpendicular and parallel susceptibility components ($\chi^{model} = \chi_{\parallel} + 2\chi_{\perp}/3$) and each component can be calculated by the van Vleck's equation (Eq. 1).

$$\chi_k = N\frac{\sum_n[E^2_{1,n,k}/kT - 2E_{2,n,k}]\exp[-E_{0,n}/kT]}{\sum_n \exp[-E_{0,n}/,kT]} \quad (n = \pm 1 \text{ to } \pm 6\ ;\ k = \parallel \text{ or } \perp). \tag{1}$$

$E_{1,n}$ and $E_{2,n}$ are the Zeeman first and second-order energy terms. The spin orbit interaction can be reduced by an orbital reduction factor (α) due to a mixture between the levels T_1 of the ^4F and a small admixture of the ^4P term. This reduction factor takes values from 1.5 in a weak field to 1 in a strong field, which reduces the effective magnetic moment [21]. Also, the spin–orbit coupling parameter (λ) is reduced by covalent effects between the metal and the O ligand. In general, the spin–orbit coupling constant for Co^{2+} in crystals is taken as $\lambda = -180\ cm^{-1}$, although in CoO compound it was estimated in $\lambda = -136\ cm^{-1}$ [22].

When the symmetry is lowered from O_h to tetragonal (i.e. D_{4h}), the triplet orbital state T_{1g} split into a singlet A_{2g} state and a doublet E_g. The effective Hamiltonian of Eq. 2 describes this situation introducing an axial distortion at zero fields (D). If this parameter is positive the ground state is the A_{2g}, while if $D < 0$ the lowest state is E_g. In general the values of D are one order of magnitude higher than λ.

$$\mathcal{H}_0 + \mathcal{H}'_{\text{Zeeman}} = \lambda\vec{L}\vec{S} + D[1 + L_z^2/\alpha^2] + \mu(-\vec{L} + 2\vec{S})\vec{H} \tag{2}$$

The part of the orbital angular momentum operators ($\vec{L}$) that is semi-diagonal in the manifold of the lowest triplet has the following components: $L_x = -\alpha' l'_x$, $L_y = -\alpha' l'_y$, $L_z = -\alpha l'_z$, where l'_x, l'_y and l'_z are the component of the angular momentum operator with quantum number equal to unity. The fine structure group levels are grouped in the subspaces of M_j ($\pm 1/2$; $\pm 3/2$; $\pm 5/2$):

$$\begin{aligned} E_4(\pm\frac{5}{2}) &= -\frac{3\alpha\lambda}{2}, \\ E_3(\pm\frac{3}{2}) &= \frac{1}{2}[D - \frac{\alpha\lambda}{2} - Q], \\ E_5(\pm\frac{3}{2}) &= \frac{1}{2}[D - \frac{\alpha\lambda}{2} + Q], \end{aligned} \tag{3}$$

where $Q = \sqrt{(D + 1/2\alpha\lambda)^2 + 6\alpha'^2\lambda^2}$, and the levels corresponding to the subspace 1/2, E_1, E_2 and E_6 are given by the roots of a cubic equation:

$$x^3 - (2\alpha + \nu)x^2 + (2\alpha\nu + \frac{3}{4}\alpha^2 - \frac{7}{2}\alpha'^2)x - \frac{3}{4}\alpha^2\nu + \frac{15}{4}3\alpha\alpha'^2 = 0 \tag{4}$$

where $\nu = D/\lambda$ and $x = E_i/\lambda$. The corresponding eigen functions are:

$$\begin{aligned} \phi^{(\pm\frac{1}{2})}_{i=1,2,6} &= a_i|\mp 1, \pm\frac{3}{2}\rangle + b_i|0, \pm\frac{1}{2}\rangle + c_i|\pm 1, \mp\frac{1}{2}\rangle, \\ \phi^{(\pm\frac{3}{2})}_{i=3,5} &= a_i|0, \pm\frac{3}{2}\rangle + b_i|\pm 1, \pm\frac{1}{2}\rangle, \\ \phi^{(\pm\frac{5}{2})}_{i=4} &= |\pm 1, \pm\frac{3}{2}\rangle, \end{aligned} \tag{5}$$

and the coefficients being defined for $i = 1$, 2 and 6 as

$$\begin{aligned} a_i &= -\frac{\sqrt{3/2}\alpha'\lambda}{3/2\alpha\lambda - E_i}b_i, \\ c_i &= \frac{\sqrt{2}\alpha'\lambda}{1/2\alpha\lambda - E_i}b_i, \\ b_i &= [\frac{3/2\alpha'^2\lambda^2}{(3/2\alpha\lambda - E_i)^2} + 1 + \frac{2\alpha'^2\lambda^2}{(1/2\alpha\lambda - E_i)^2}]^{-1/2}, \end{aligned} \tag{6}$$

and for $i = 3$ and 5 are:

$$\begin{aligned} a_i &= -\frac{\sqrt{3/2}\alpha'\lambda}{D - E_i}b_i, \\ b_i &= [\frac{3/2\alpha'^2\lambda^2}{(D - E_i)^2} + 1]^{-1/2}, \end{aligned} \tag{7}$$

In conclusion, the model gives an estimation of the effective magnetic moment where the parameters to define are: λ, α, α', D and T. For example, fixing the temperature, it is possible to study the μ_{eff}^{model} dependence with the crystal field parameter D. On the other hand, fixing D, we can study the μ_{eff}^{model} behavior with temperature. The $\mu_{eff}^{model} = \sqrt{(3k/N_A\mu_B^2)\chi^{model}T}$ can be calculated computing the magnetic susceptibility by using the van Vleck equation and the energy levels including axial local crystal field distortion (Eqs. (1)–(7)) and following the steps described in Refs. [14,20,23].

3.2. Comparing the experimental results with the model

As the D parameter is the axial crystal field of a cubic field, the Ba_2CoWO_6 system have $D = 0\ cm^{-1}$ because D is the axial distortion of a cubic system, this null value for the parameter does not occur in the other two systems (Ca and Sr).

In Fig. 4 we represent three sets of μ_{eff}^{model} vs. D curves at $T = 300$ K (a, b and c). Only $D > 0$ values are plotted because the

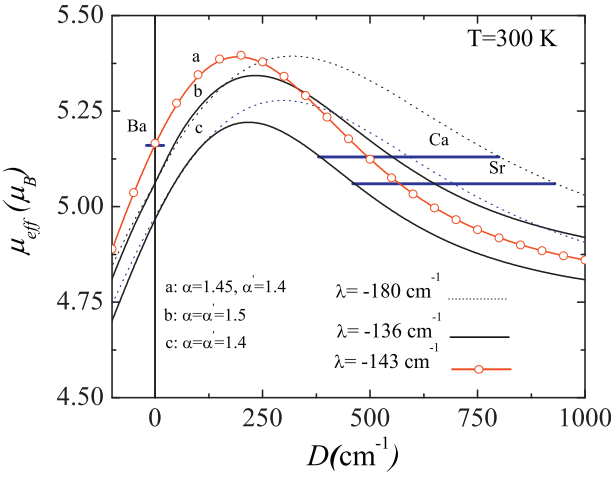

Fig. 4. Effective magnetic moment (μ_{eff}) as a function of the crystal field distortion parameter (D). Experimental μ_{eff} values at 300 K and $H = 5$ kOe are represented by horizontal lines (blue) and labelled with Ba, Ca or Sr corresponding to the A cation in the double perovskite. Three sets (a, b and c) of μ_{eff}^{model} vs. D curves are shown to compare with the experimental data. In b and c, solid and dotted lines are calculated with $\lambda = -136$ and $-180\ cm^{-1}$ respectively. In b, $\alpha = \alpha' = 1.5$ and in c is $\alpha = \alpha' = 1.4$. The μ_{eff}^{model} of a curve (line with circles in red) has been computed with $\lambda = -143\ cm^{-1}$, $\alpha = 1.45$ and $\alpha' = 1.40$ in order to describe the experimental μ_{eff} value of the Ba compound at 300 K. The intersection between the experimental values with this a curve can display the corresponding D values for the Ca and Sr cases. (For interpretation of the references to colour in this figure legend, the reader is referred to the web version of this article.)

negative crystal field parameter gives lower effective magnetic moments than the experimental μ_{eff} data. In the plot, to illustrate the behavior of the model, two examples with $\alpha = \alpha'$ (b and c) can be appreciated. Also, we use two representative spin–orbit interaction values: (i) $\lambda = -180\ cm^{-1}$, which is a normally used value to describe compounds with Co^{2+} ions [20], and (ii) $-136\ cm^{-1}$, which is used in more covalent oxides as CoO [22]. In particular, for these two λ values, we plot b curve using $\alpha = \alpha' = 1.5$ and $\alpha = \alpha' = 1.4$ in c curve, both values are associated with weak crystal field. This graph is also an indication of the different possible ranges of each parameter of the model. The resulting μ_{eff}^{model} vs. D curves show the same tendency: starting at $D = 0\ cm^{-1}$ with a finite μ_{eff}^{model} value, which increases until to reach a maximum between $1 \leq |D/\lambda| \leq 2$ and for larger D, the effective magnetic moment decreases asymptotically. At low D values, both curves with different λ are practically coincident but this are shifted at higher D. With $\alpha = \alpha'$, the model cannot explain the experimental μ_{eff} for the Ba case, which is higher than the values obtained in curves b and c. At $D = 0\ cm^{-1}$, the experimental μ_{eff} value for the Ba double perovskite is reached using $\lambda = -143\ cm^{-1}$ and $\alpha \neq \alpha'$, with $\alpha = 1.45$ and $\alpha' = 1.40$ (see curve a). This curve let us to infer the corresponding D values for the Sr and Ca double perovskite, which are the intersections between the a curve and the experimental μ_{eff} values at 300 K represented by horizontal lines in Fig. 4 (their wide are only indicative between the calculated curves).

We compute the experimental effective magnetic moment as a function of temperature as: $\mu_{eff}(T) = \sqrt{(3k/N_A\mu_B^2)\chi(T+\theta)}$ where χ is the experimental magnetic susceptibility and θ is the Curie–Weiss constant obtained by the Curie–Weiss law fitted at high temperature (the θ values were calculated in previous sections and the data are in Table 1). In Fig. 5, we represent with symbols the experimental effective magnetic moment as a function of temperature for the different double perovskites at 5 and 50 kOe of magnetic field.

Now, to describe these experimental values, we calculate $\mu_{eff}^{model}(T)$ using $\lambda = -143\ cm^{-1}$ for the double perovskite system; and $D = 0\ cm^{-1}$, $D = 487\ cm^{-1}$ and $D = 557\ cm^{-1}$ for Ba, Ca and Sr respectively. These parameters have been obtained from the evaluation of the room temperature data, which were analyzed in Fig. 4. During the calculus of each curve, we fix these model parameters (λ and D), while α and α' are free in order to obtain the best adjust between the experimental data and the model. The calculated $\mu_{eff}^{model}(T)$ values are shown with solid lines in Fig. 5 and the set of parameters that describe each curve are in Table 1. Our previous observation that the μ_{eff} is reduced when ⟨Co–O⟩ is diminished and that this μ_{eff} dependence can be associated with crystal field effects, it is completely confirmed by our calculus. The cobalt effective magnetic moment in double perovskites principally changes by crystal field effects. Indeed, the model describes the experimental effective magnetic moment computed at two different magnetic field using the same crystal field distortion and spin orbit interaction value. In particular, we remark that the axial crystal field distortion parameters that describe perfectly the experimental situation are $D(Ba) \approx 0\ cm^{-1}$, $D(Ca) \approx 487\ cm^{-1}$ and $D(Sr) \approx 557\ cm^{-1}$.

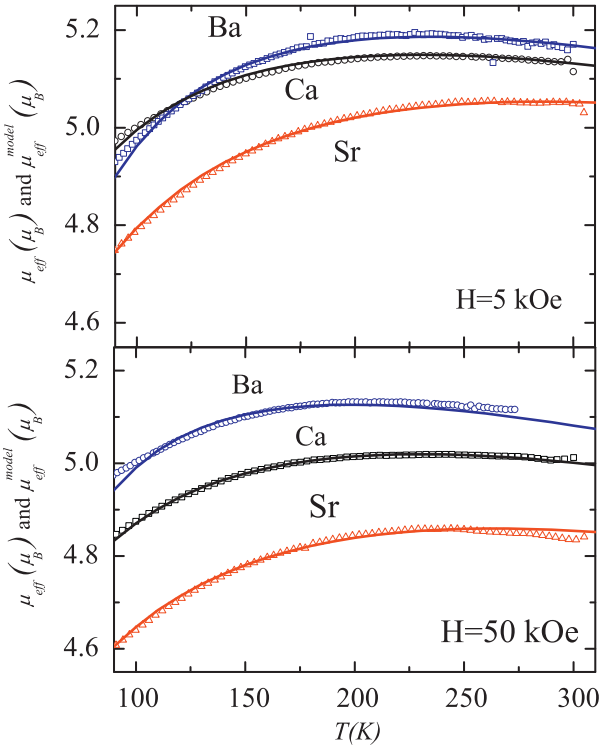

Fig. 5. $\mu_{eff}(T)$ values for A = Ba (□, blue), Ca (○, black) and Sr(△, red) in the double perovskites A_2CoWO_6. In the top are the experimental data taken at 5 kOe, while in the bottom are the data at 50 kOe. Solid lines show the calculus of $\mu_{eff}^{model}(T)$ as a function of temperature for each case. All the calculated curves are with $\lambda = -143\ cm^{-1}$ and $D = 0\ cm^{-1}$, $D = 487\ cm^{-1}$ and $D = 557\ cm^{-1}$ for Ba, Ca and Sr respectively. The α and α' values used for the calculus in each case are in Table 1.

4. Conclusions

We report magnetic susceptibility experiments in the paramagnetic region about Ca_2CoWO_6, Sr_2CoWO_6 and Ba_2CoWO_6 double perovskites. The effective magnetic moment (μ_{eff}) of Co^{2+}, partially unquenched, increases with the mean ⟨Co–O⟩ distance indicating the presence of crystal field effects on the Co^{2+} environment. A simple model to describe the magnetic susceptibility with octahedral crystal field distortion describes the behavior of the effective magnetic moment in practically all the experimental temperature range in the double cobalt perovskites with A = Ca, Sr and Ba. The best $\lambda = -143\ cm^{-1}$ value that describe the experimental situation indicates an important covalence in this kind of oxides.

Acknowledgments

C.A.L. and M.E.S. thank to CONICET for their fellowships. R.D.S. acknowledges financial support of ANPCYT (PICT 07-0892 and PAE 063-PME20), and SEPCyT-UNCu (06/C324). The authors acknowledge to Prof. J.C. Pedregosa for the fruitful discussion. J.C. and R.D.S are members of CONICET.

References

[1] K.I. Kobayashi, T. Kimura, H. Sawada, K. Terakura, Y. Tokura, Nature 395 (1998) 677–680.
[2] D. Niebieskikwiat, R.D. Sánchez, A. Caneiro, L. Morales, M. Vásquez-Mansilla, F. Rivadulla, L.E. Hueso, Phys. Rev. B 62 (5) (2000) 3340–3345.
[3] J.B. Philipp, D. Reisinger, M. Schonecke, M. Opel, A. Marx, A. Erb, L. Alff, R. Gross, J. Appl. Phys. 93 (10) (2003) 6853–6855.
[4] D. Niebieskikwiat, A. Caneiro, R.D. Sánchez, J. Fontcuberta, Phy. Rev. B 64 (18) (2001), 180406(R) 1804061-1804064.
[5] M. Bibes, K. Bouzehouane, M. Besse, A. Barthélémy, S. Fusil, M. Bowen, P. Seneor, J.P. Contour, A. Fert, Appl. Phys. Lett. 83 (13) (2003) 2629–2631.
[6] H. Asano, N. Koduka, K. Imaeda, M. Sugiyama, M. Matsui, IEEE Trans. Magn. 41 (10) (2005) 2811–2813.
[7] S.A. Wolf, D.D. Awschalom, R.A. Buhrman, J.M. Daughton, S. Von Molnár, M.L. Roukes, A.Y. Chtchelkanova, D.M. Treger, Science 294 (5546) (2001) 1488–1495, I. Žuti, J. Fabian, S.D. Sarma, Rev. Mod. Phys. 76 (2) (2004) 323–410.
[8] J. Nogués, I.K. Schuller, J. Magn. Magn. Mater 192 (2) (1999) 203–232, A.E. Berkowitz, K. Takano, J. Magn. Magn. Mater. 200 (1) (1999) 552–570.
[9] M.J. Martínez-Lope, J.A. Alonso, M.T. Casais, M.T. Fernández-Díaz, Z. Naturforsch. 58b (2003) 127–132.

[10] M.C. Viola, M.J. Martínez-Lope, J.A. Alonso, P. Velasco, J.L. Martínez, J.M. De Paoli, S. Pagola, J.C. Pedregosa, M.T. Fernández-Díaz, R.E. Carbonio, Chem. Mater. 15 (2003) 1655–1663.
[11] M.J. Martínez-Lope, J.A. Alonso, M.T. Casais, M.T. Fernández-Díaz, Eur. J. Inorg. Chem. 9 (2002) 2463–2469.
[12] S.Z. Tian, J.C. Zhao, C.D. Qiao, X.L. Ji, B.Z. Jiang, Mater. Lett. 60 (2006) 2747–2750.
[13] V.C. Fuertes, M.C. Blanco, D.G. Franco, J.M. De Paoli, R.D. Sánchez, R.E. Carbonio, Mater. Res. Bull. 46 (2011) 62–69.
[14] A. Bose, A.S. Chakravarty, R. Chatterjee, Proc. R. Soc. A 261 (1961) 43.
[15] M.C. Viola, M.J. Martínez-Lope, J.A. Alonso, P. Velasco, J.L. Martínez, J.C. Pedregosa, R.E. Carbonio, M.T. Fernández-Díaz, Chem. Mater. 14 (2002) 812–818.
[16] R.M. Pinacca, M.C. Viola, J.C. Pedregosa, A. Mu ñoz, J.A. Alonso, J.L. Martínez, R.E. Carbonio, Dalton Trans. 3 (2005) 447–451.
[17] Y. Hinatsu, Y. Doi, J. Solid State Chem. 179 (2006) 2084–2090.
[18] M.S. Augsburger, M.C. Viola, J.C. Pedregosa, A. Mu ñoz, J.A. Alonso, R.E. Carbonio, J. Mater. Chem. 15 (2005) 993–1001.
[19] C.A. López, M.C. Viola, J.C. Pedregosa, R.E. Carbonio, R.D. Sánchez, M.T. Fernández-Díaz, J. Solid State Chem. 181 (2008) 3095–3102.
[20] A.S. Chakravarty, Introduction to the Magnetic Properties of Solids, Wiley, New York, 1980.
[21] F. Lloret, M. Julve, J. Cano, R. Ruíz-García, E. Pardo, Inorg. Chim. Acta 361 (12–13) (2008) 3432–3445.
[22] P. Cossee, Mol. Phys. 3 (2) (1960) 125–129.
[23] A. Abragam, M.H.L. Pryce, Proc. R. Soc. A 206 (1951) 173.